International Journal of Applied Electromagnetics and Mechanics 34 (2010) 33–48
DOI 10.3233/JAE-2010-1085
IOS Press

Image reconstruction of inhomogeneous biaxial dielectric cylinders buried in a slab medium

Chi Hsien Sun, Chien-Ching Chiu* and Chun Jen Lin
Electrical Engineering Department, Tamkang University, Tamsui, Taipei, Taiwai

Abstract. The image reconstruction of inhomogeneous biaxial dielectric cylinders buried in a slab medium is investigated. A biaxial dielectric cylinder of unknown permittivities buried in a slab scatters a group of unrelated incident waves from outside. The scattered field is recorded outside the slab. By proper arrangement of the various unrelated incident fields, the difficulties of ill-posedness and nonlinearity are circumvented, and the permittivity distribution can be reconstructed through simple matrix operations. The algorithm is based on the moment method and the unrelated illumination method. Numerical results are given to demonstrate the capability of the inverse algorithm. Good reconstructed results are obtained even in the presence of additive Gaussian random noise in measured data. In addition, the effect of noise on the reconstruction result is also investigated.

1. Introduction

In inverse scattering, one attempts to infer the profile of an object from the measurement data collected away from the scatterer. Needless to say, this is very important for a number of sensing and remote sensing applications [1–13]. For instance, it finds applications in nondestructive testing, geophysical probing, microwave and ultrasonic medical imaging, buried-object detection, radar imaging and target identification. The two main difficulties for the inverse problems are highly ill-posed and nonlinearity. Ill-posedness means that a small error in the measured field data may cause a large error in the reconstructed result. For inverse scattering solved by discrete matrix equations, the ill-condition property of associated matrices reflects the ill-posedness of inverse scattering. Ill-posedness may be caused by the natural limitation for propagating waves to carry high spatial frequency information or by the limited ability of the reconstruction algorithm to make efficient use of the measured data. This problem is also ill-posed due to the face that the kernel of the integral is a smoothing function. Another one is nonlinearity. The inverse scattering problem is nonlinear in nature because in involves the product of two unknowns, the electrical property of object, and the electric field within the object. Especially in inverse problems of a slab medium, the interaction between the interface of the three layers and the object, which leads to the complicated Green's function for this three layer problem. Owing to the difficulties in computing the Green's function by a numerical method, the problem of inverse scattering in a slab has seldom been tackled. Most papers emphasize on the reconstruction of the second layer profile in the three

*Corresponding author. E-mail: chiu@ee.tku.edu.tw.

1383-5416/10/$27.50 © 2010 – IOS Press and the authors. All rights reserved

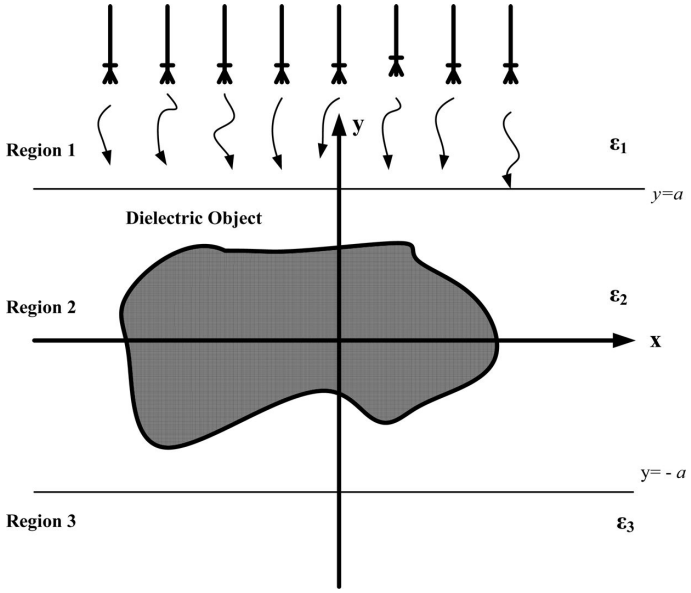

Fig. 1. Geometry of problem in the (x,y) plane.

layer structures [11–14]. However, only a few papers deal with the reconstruction of buried perfectly conducting objects in the three layer structures [15,16].

At the same time, advanced composite materials are increasingly popular in industrial and military application due to their superior properties in strength and stiffness. The electromagnetic inverse scattering of advanced composite materials has been a subject of considerable importance in various area of technology. However, the composite materials are electrically anisotropic. The permittivity of these materials depends on the chosen coordinates. This problem is more difficult and complex than that of isotropic materials. To the best of our knowledge, there is still no investigation on the electromagnetic imaging of inhomogeneous dielectric cylinders buried in a slab medium.

In this paper, the inverse scattering of buried inhomogeneous biaxial dielectric cylinders is investigated. An efficient algorithm is proposed to reconstruct the permittivity distribution of the objects by using only the scattered field measured outside. The algorithm is based on the unrelated illumination method [9,17]. In Section 2, the theoretical formulation for electromagnetic inverse scattering is presented. Numerical results for objects of different permittivity distributions are given in Section 3. Finally, conclusions are drawn in Section 4.

2. Theoretical formulation

2.1. Direct problem

Let us consider biaxial dielectric cylinders buried in a lossless homogeneous three-layer background as shown in Fig. 1, where $\varepsilon_i \;\; i = 1, 2, 3$, denote the permittivities in each region. The permeability is μ_0 for all material including the scatterers. The axis of the buried cylinder is the z-axis; that is, the properties of the scatterer may vary with the transverse coordinates only. The permittivity tensors $\bar{\bar{\varepsilon}}_r$ of

the dielectric objects are represented by diagonal matrix in the Cartesian coordinate system

$$\bar{\bar{\varepsilon}}_r(x,y) = \begin{bmatrix} \varepsilon_a(x,y) & 0 & 0 \\ 0 & \varepsilon_b(x,y) & 0 \\ 0 & 0 & \varepsilon_c(x,y) \end{bmatrix}_{xyz} \tag{1}$$

The object is illuminated by the following two different polarized incident waves.

1. TM Waves: A group of unrelated incident wave with electric field parallel to the z-axis (i.e., transverse magnetic) is illuminated upon the scatterers. Owing to the interface between region 1 and 2, the incident waves generate two waves that would exist in the absence of the scatterer: reflected waves (for $y \geqslant a$) and transmitted waves (for $y < -a$). Let the unperturbed field be represented by

$$\vec{E}^{\,i}(x,y) = \begin{cases} \left(E_z^i\right)_1(x,y)\hat{z}, & y \geqslant a, \\ \left(E_z^i\right)_2(x,y)\hat{z}, & a > y > -a, \\ \left(E_z^i\right)_3(x,y)\hat{z}, & y \leqslant -a. \end{cases} \tag{2}$$

Then the internal total electric field inside the biaxial object, $\vec{E}(x,y) = E(x,y)\hat{z} = [E_z^i(x,y) + E_z^s(x,y)]\hat{z}$, can be expressed by the following integral equation:

$$E_z^i\left(\vec{r}\right) = \int_s G\left(\vec{r},\vec{r}\,'\right) k_2^2 \left[\varepsilon_c\left(\vec{r}\,'\right) - 1\right] E_z\left(\vec{r}\,'\right) ds' + E_z\left(\vec{r}\right), \quad a > y > -a \tag{3}$$

The scattered field, $\vec{E}_s(x,y) = E_z^s(x,y)\hat{z}$, can be expressed as

$$E_z^s\left(\vec{r}\right) = -\int_s G\left(\vec{r},\vec{r}\,'\right) k_2^2 \left[\varepsilon_c\left(\vec{r}\,'\right) - 1\right] E_z\left(\vec{r}\,'\right) ds' \tag{4}$$

with

$$G(x,y;x',y') = \begin{cases} G_{1s}(x,y:x',y'), & y \geqslant a, \\ G_{2s}(x,y;x',y'), & -a < y < a, \\ G_{3s}(x,y;x',y'), & y \leqslant -a, \end{cases} \tag{5a}$$

$$G_{1s}(x,y;x',y') = \frac{1}{2\pi}\int_{-\infty}^{\infty} j e^{-j\gamma_1(y-a)} \frac{(\gamma_2+\gamma_3)\,e^{j\gamma_2(y'+a)} + (\gamma_2-\gamma_3)\,e^{-j\gamma_2(y'+a)}}{(\gamma_1+\gamma_2)(\gamma_2+\gamma_3)\,e^{j\gamma_2(2a)} + (\gamma_1-\gamma_2)(\gamma_2-\gamma_3)\,e^{-j\gamma_2(2a)}} e^{-j\alpha(x-x')} d\alpha, \tag{5b}$$

$$G_{2s}(x,y;x',y') = G_{2sf}(x,y;x',y') + G_{2ss}(x,y;x',y') \tag{5c}$$

$$G_{3s}(x,y;x',y') = \frac{1}{2\pi}\int_{-\infty}^{\infty} j e^{j\gamma_1(y+a)} \frac{(\gamma_1+\gamma_2)\,e^{-j\gamma_2(y'-a)} + (\gamma_2-\gamma_1)\,e^{j\gamma_2(y'-a)}}{(\gamma_1+\gamma_2)(\gamma_2+\gamma_3)\,e^{j\gamma_2(2a)} + (\gamma_1-\gamma_2)(\gamma_2-\gamma_3)\,e^{-j\gamma_2(2a)}} e^{-j\alpha(x-x')} d\alpha, \tag{5d}$$

where

$$G_{2sf}(x,y;x',y') = \frac{j}{4}H_0^{(2)}\left(k_2\sqrt{(x-x')^2+(y-y')^2}\right)$$

$$G_{2ss}(x,y;x',y') = \frac{1}{2\pi}\int_{-\infty}^{\infty}\frac{j}{2\gamma_2}\left\{\left[\frac{(\gamma_2-\gamma_1)(\gamma_2-\gamma_3)\left[e^{-j\gamma_2[|y-y'|+2a]}+e^{j\gamma_2[|y-y'|-2a]}\right]}{(\gamma_1+\gamma_2)(\gamma_2+\gamma_3)e^{j\gamma_2(2a)}+(\gamma_1-\gamma_2)(\gamma_2-\gamma_3)e^{-j\gamma_2(2a)}}\right]\right.$$
$$\left.+\left[\frac{(\gamma_2-\gamma_1)(\gamma_2+\gamma_3)e^{j\gamma_2(y+y')}+(\gamma_2-\gamma_3)(\gamma_1+\gamma_2)e^{-j\gamma_2(y+y')}}{(\gamma_1+\gamma_2)(\gamma_2+\gamma_3)e^{j\gamma_2(2a)}+(\gamma_1-\gamma_2)(\gamma_2-\gamma_3)e^{-j\gamma(2a)}}\right]\right\}$$
$$e^{-j\alpha(x-x')}d\alpha$$

$$\gamma_i^2 = k_i^2-\alpha^2, \quad i=1,\,2,\,3 \quad Im(\gamma_i)\leqslant 0, \quad a>y'>-a.$$

Here k_i denotes the wave number in region i. $G(x,y;x',y')$ is the Green's function, which can be obtained by the Fourier transform [2]. $H_0^{(2)}$ is the Hankel function of the second kind of order 0. For numerical implementation of Green's function, we might face some difficulties in calculating this function. This Green's function is in the form of an improper integral, which must be evaluated numerically. However, the integral converges very slowly when (x,y) and (x',y') approach the interface $y=a$. Fortunately we find that the integral in G_{1s}, G_{2s} and G_{3s} may be rewritten as a closed-form term plus a rapidly converging integral [2]. Thus the whole integral in the Green's function can be calculated efficiently.

2. TE Waves: A group of unrelated incident wave with magnetic field parallel to the z-axis (i.e., transverse electric) is illuminated upon the object. Owing to the interface, the incident plane wave generates three waves that would exist in the absence of the conducting object. Let the unperturbed field be represented by

$$\vec{E}^{\,i}(x,y) = \begin{cases} \left(E_x^i\right)_1(x,y)\hat{x}+\left(E_y^i\right)_1(x,y)\hat{y}, & y\geqslant a,\\ \left(E_x^i\right)_2(x,y)\hat{x}+\left(E_y^i\right)_2(x,y)\hat{y}, & a>y>-a,\\ \left(E_x^i\right)_3(x,y)\hat{x}+\left(E_y^i\right)_3(x,y)\hat{y}, & y\leqslant -a. \end{cases} \tag{6}$$

Owing to the coupling between E_x and E_y, the equations governing the result total field in the TE case are more complicated than those in the TM case. By using Hertz vectorial potential techniques [18], the internal total electric field

$$\vec{E}(x,y) = E_x(x,y)\hat{x}+E_y(x,y)\hat{y} = (E_x^i+E_x^s)\hat{x}+(E_y^i+E_y^s)\hat{y}$$

and the external scattered field,

$$\vec{E}^{\,s}(x,y) = E_x^s(x,y)\hat{x}+E_y^s(x,y)\hat{y}$$

can be expressed by the following equations:

$$E_x(\vec{r}) = -\left(\frac{\partial^2}{\partial x^2}+k_2^2\right)\left[\int_s G(\vec{r},\vec{r}\,')(\varepsilon_a(\vec{r}\,')-1)E_x(\vec{r}\,')ds'\right]$$
$$-\frac{\partial^2}{\partial x\partial y}\left[\int_s G(\vec{r},\vec{r}\,')(\varepsilon_b(\vec{r}\,')-1)E_y(\vec{r}\,')ds'\right]+E_x^i(\vec{r}) \tag{7}$$

$$E_y(\vec{r}) = -\frac{\partial^2}{\partial x \partial y}\left[\int_s G(\vec{r},\vec{r}')(\varepsilon_a(\vec{r}')-1)E_x(\vec{r}')ds'\right] - \left(\frac{\partial^2}{\partial y^2}+k_2^2\right)\left[\int_s G(\vec{r},\vec{r}')(\varepsilon_b(\vec{r}')-1)E_y(\vec{r}')ds'\right] + E_y^i(\vec{r}) \tag{8}$$

$$E_x^s(\vec{r}) = -\left(\frac{\partial^2}{\partial x^2}+k_2^2\right)\left[\int_s G(\vec{r},\vec{r}')(\varepsilon_a(\vec{r}')-1)E_x(\vec{r}')ds'\right] - \frac{\partial^2}{\partial x \partial y}\left[\int_s G(\vec{r},\vec{r}')(\varepsilon_b(\vec{r}')-1)E_y(\vec{r}')ds'\right] \tag{9}$$

$$E_y^s(\vec{r}) = -\frac{\partial^2}{\partial x \partial y}\left[\int_s G(\vec{r},\vec{r}')(\varepsilon_a(\vec{r}')-1)E_x(\vec{r}')ds'\right] - \left(\frac{\partial^2}{\partial y^2}+k_2^2\right)\left[\int_s G(\vec{r},\vec{r}')(\varepsilon_b(\vec{r}')-1)E_y(\vec{r}')ds'\right] \tag{10}$$

For the direct problem, the scattered field is computed by giving the permittivity distribution of the biaxial objects buried in a slab medium. This can be achieved by using Eq. (3) to solve the total field inside the object $\bar{E}$ and calculating $\bar{E}^s$ by Eq. (4) for the TM waves. Similarly, this can be achieved by using Eqs (7) and (8) to solve the total field inside the object $\bar{E}$ and calculating $\bar{E}^s$ by Eqs (9) and (10) for the TE waves. For numerical implementation of the direct problem, the dielectric objects are divided into N sufficient small cells. Thus the permittivity and the total field within each cell can be taken as constants. Let ε_{an}, ε_{bn} and ε_{cn} denote the x, y and z component of relative permittivity in the nth cell. Then the moment method is used to solve Eqs (3), (4), and Eqs (7)–(10) with a pulse basis function for expansion and point matching for testing [19]. Thus the following matrix equations can be obtained:

$$(E_z^i) = [[G_2][\tau_c] + [I]]\ (E_z) \tag{11}$$

$$(E_z^s) = -[G_1]\,[\tau_c]\,(E_z) \tag{12}$$

$$\begin{pmatrix} E_x^i \\ E_y^i \end{pmatrix} = \left\{ \begin{bmatrix} [G_3] & [G_4] \\ [G_4] & [G_5] \end{bmatrix} \begin{bmatrix} [\tau_a] & 0 \\ 0 & [\tau_b] \end{bmatrix} + \begin{bmatrix} [I] & 0 \\ 0 & [I] \end{bmatrix} \right\} \begin{pmatrix} E_x \\ E_y \end{pmatrix} \tag{13}$$

$$\begin{pmatrix} E_x^s \\ E_y^s \end{pmatrix} = \left\{ - \begin{bmatrix} [G_6] & [G_7] \\ [G_7] & [G_8] \end{bmatrix} \begin{bmatrix} [\tau_a] & 0 \\ 0 & [\tau_b] \end{bmatrix} \right\} \begin{pmatrix} E_x \\ E_y \end{pmatrix} \tag{14}$$

where (E_x^i), (E_y^i), and (E_z^i) represent the N-element incident field column vectors and, (E_x), (E_y), and (E_z) are the N-element total field column vectors. (E_x^s) , (E_y^s), and (E_z^s) denote the M-element scattered field column vectors. Here M is the number of measurement points. The matrices [G_2], [G_3], [G_4], and [G_5] are $N \times N$ square matrices. [G_1], [G_6], [G_7], and [G_8] are $M \times N$ matrices. The element in matrices [G_i], $i = 1, 2, 3 \ldots 8$ can be obtained by tedious mathematic manipulation (see Appendix). $[\tau_a]$,$[\tau_b]$ and $[\tau_c]$ are $N \times N$ diagonal matrixes whose diagonal element are formed from the permittivities of each cell minus one. [I] is a identity $N \times N$ matrix. We can solve the direct problem for the TM case by using Eqs (11) and (12). Similarly, the direct problem for TE case can be solved by using Eqs (13) and (14).

2.2. Inverse problem

We consider the following inverse problem: the permittivity distribution of the biaxial dielectric objects is to be computed by the knowledge of the scattered field measured in region 1. Note that the only unknown permittivities are $\varepsilon_c(r)$ for the TM case, and similarly the only unknown permittivities are $\varepsilon_a(r)$ and $\varepsilon_b(r)$ for the TE case. In the inversion procedure, we choose N different incident column vectors for the TM case and $2N$ different incident column vectors for the TE case. Then Eqs (11)–(14) can be expressed as

$$[E_z^i] = [[G_2][\tau_c] + [I]]\ [E_z] \tag{15}$$

$$[E_z^s] = -[G_1]\ [\tau_c]\ [E_z] \tag{16}$$

$$[E_t^i] = [[G_{t1}][\tau_t] + [I_t]]\ [E_t] \tag{17}$$

$$[E_t^s] = -\,[G_{t2}]\ \ [\tau_t]\ \ [E_t] \tag{18}$$

where

$$[E_t^i] = \begin{bmatrix} E_x^i \\ E_y^i \end{bmatrix} \quad [E_t] = \begin{bmatrix} E_x \\ E_y \end{bmatrix} \quad [E_t^s] = \begin{bmatrix} E_x^s \\ E_y^s \end{bmatrix}$$

$$[G_{t1}] = \begin{bmatrix} [G3]\ [G4] \\ [G4]\ [G5] \end{bmatrix}, \quad [G_{t2}] = \begin{bmatrix} [G6]\ [G7] \\ [G7]\ [G8] \end{bmatrix}$$

$$[\tau_t] = \begin{bmatrix} [\tau_a]\ 0 \\ 0\ [\tau_b] \end{bmatrix}, \qquad [I_t] = \begin{bmatrix} [I]\ 0 \\ 0\ [I] \end{bmatrix}$$

Here $[E_z^i]$ and $[E_z]$ are both $N \times N$ matrices. $[E_z^s]$ is a $M \times N$ matrix. $[E_t^i]$ and $[E_t]$ are both $2N \times 2N$ matrices. $[E_t^s]$ is a $M \times 2N$ matrix. It is worth mentioning that other than matrices $[G_1]$ and $[G_{t2}]$, the matrices $[G_2][\tau_c] + [I]$ and $[G_{t1}][\tau_t] + [I_t]$ are always well-posed ones in any case. Therefore, by first solving $[E_z^]$ in Eq. (15) as well as $[E_t^]$ in Eq. (17) and substituting into Eqs (16) and (18), respectively. Then $[\tau_c]$ and $[\tau_t]$ can be found by solving the following equations:

$$[\Psi_z][\tau_c] = [\Phi_z] \tag{19}$$

$$[\Psi_t][\tau_t] = [\Phi_t] \tag{20}$$

where

$$[\Phi_z] = -[E_z^s][E_z^i]^{-1}$$

$$[\Psi_z] = [E_z^s][E_z^i]^{-1}[G_2] + [G_1]$$

$$[\Phi_t] = -[E_t^s][E_t^i]^{-1}$$

$$[\Psi_t] = [E_t^s][E_t^i]^{-1}[G_{t1}] + [G_{t2}]$$

From Eq. (19), all the diagonal elements in the matrix $[\tau_c]$ can be determined by comparing the element with the same subscripts, which may be any row of both $[\Psi_z]$ and $[\Phi_z]$:

$$(\tau_c)_{nn} = \frac{(\Phi_z)_{mn}}{(\Psi_z)_{mn}} \tag{21}$$

Similarly, from Eq. (20),

$$(\tau_a)_{nn} = \frac{(\Phi_t)_{mn}}{(\Psi_t)_{mn}},\ n \leqslant N \tag{22}$$

or

$$(\tau_b)_{(n-N)(n-N)} = \frac{(\Phi_t)_{mn}}{(\Psi_t)_{mn}},\ n \geqslant N+1 \tag{23}$$

Note that there are a total of M possible values for each element of τ_a, τ_b, and τ_c. Therefore, the average value of these M data is computed and chosen as final reconstruction result in the simulation.

In the above derivation, the key problem is that the incident matrices $[E_z^i]$ and $[E_t^i]$ must not be a singular matrix, i.e., all the incident column vectors that form the $[E_z^i]$ and $[E_t^i]$ matrices, must be linearly unrelated. Thus, if the object is illuminated by a group of unrelated incident waves, it is possible to reconstruct the permittivity distribution of the objects. Note that when the number of cells becomes very large; it is difficult to make such a great number of independent measurements. In such a case, some regularization methods must be used to overcome the ill-posedness.

3. Numerical results

In this section, we report some numerical results obtained by computer simulations using the method described in the Section 2. Let us Consider a lossless three- layer structure ($\sigma_1 = \sigma_2 = \sigma_3 = 0$) and the width of the second layer is 0.2 m. The permittivity in each region is characterized by, $\varepsilon_1 = \varepsilon_0$, $\varepsilon_2 = 2.25\varepsilon_0$ and $\varepsilon_3 = \varepsilon_0$ respectively, as shown in Fig. 1. The frequency of the incident wave is chosen as 3GHz. and the number of illuminations is the same as that of cells. The incident waves are generated by numerous groups of radiators operated simultaneously.

Each group of radiators is restricted to transmit a narrow-beamwidth pattern that can be implemented by antenna array techniques. By changing the beam direction and tuning the phase of each group of radiators, one can focus all the incident beams in turn at each cell of the object. This procedure is named "beam focusing" [9]. Note that this focusing should be set when the scatterer is absent. Clearly, an incident matrix formed in this way is diagonally dominant and its inverse matrix exists. The transmitting antenna array has 1340 elements in order to achieve the EM wave of beamwidth 0.0176°, which is required to focus on the desired cell of 0.25cm for the cylinder in region 2 for the case of 3GHz assumed in this study. The spacing of the equally separated array elements is $\frac{\lambda}{2}$, and the antenna array is set 200 cm (20λ) away from the interface between region1 and region2 to illuminate to scatterer. The measurement is taken from 0.4 m to -0.4 m in region 1 at equal spacing. The number of measurement points is set to be 9 for each illumination. For avoiding trivial inversion of finite dimensional problems, the discretization number for the direct problem is four times that for the inverse problem in our numerical simulation.

In the first example, the buried cylinder with a 62.5 mm $\times$ 10 mm rectangular cross section is discretized into 25 $\times$ 4 cells, and the corresponding dielectric permittivities are plotted in Fig. 2. The model is

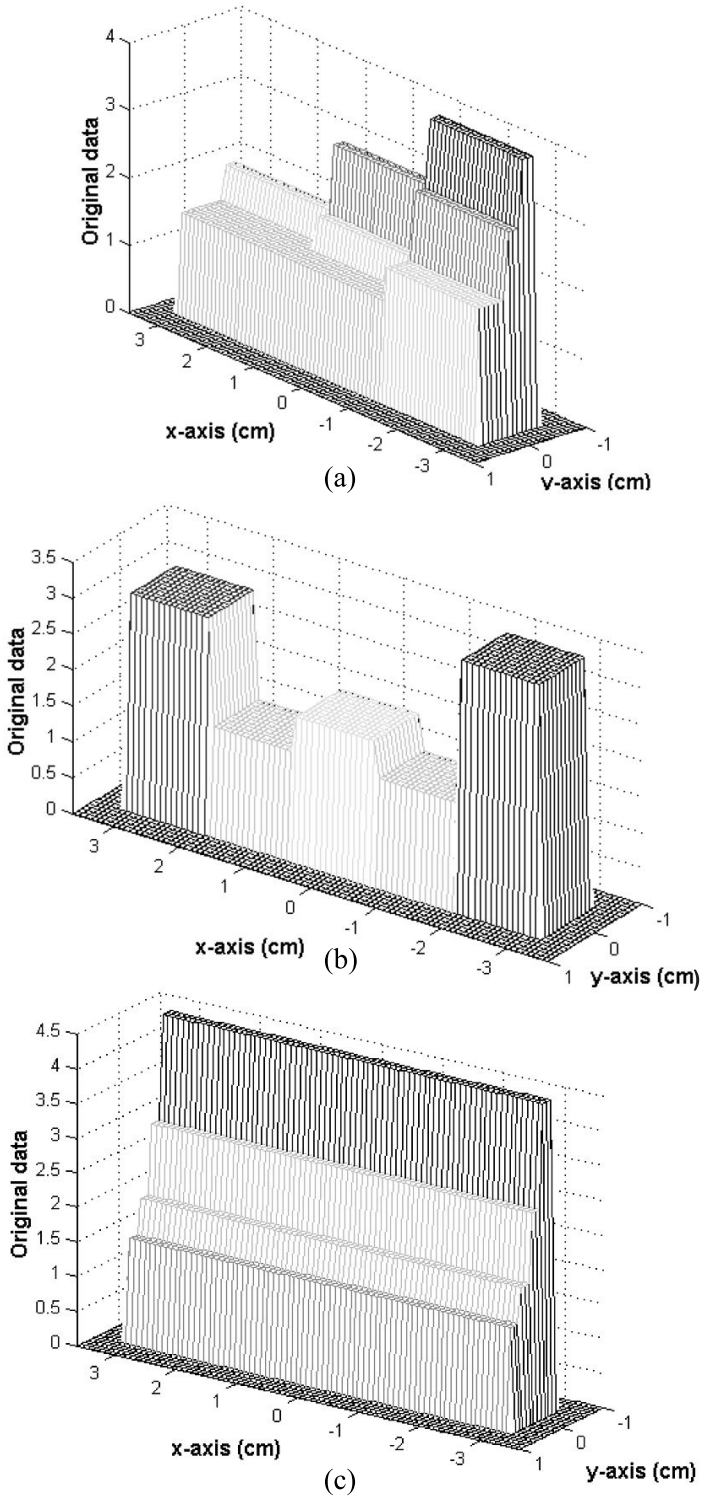

Fig. 2. Original relative permittivity distribution for example 1, (a)$\varepsilon_a\,(x,y)$, (b)$\varepsilon_b\,(x,y)$, (c)$\varepsilon_c\,(x,y)$.

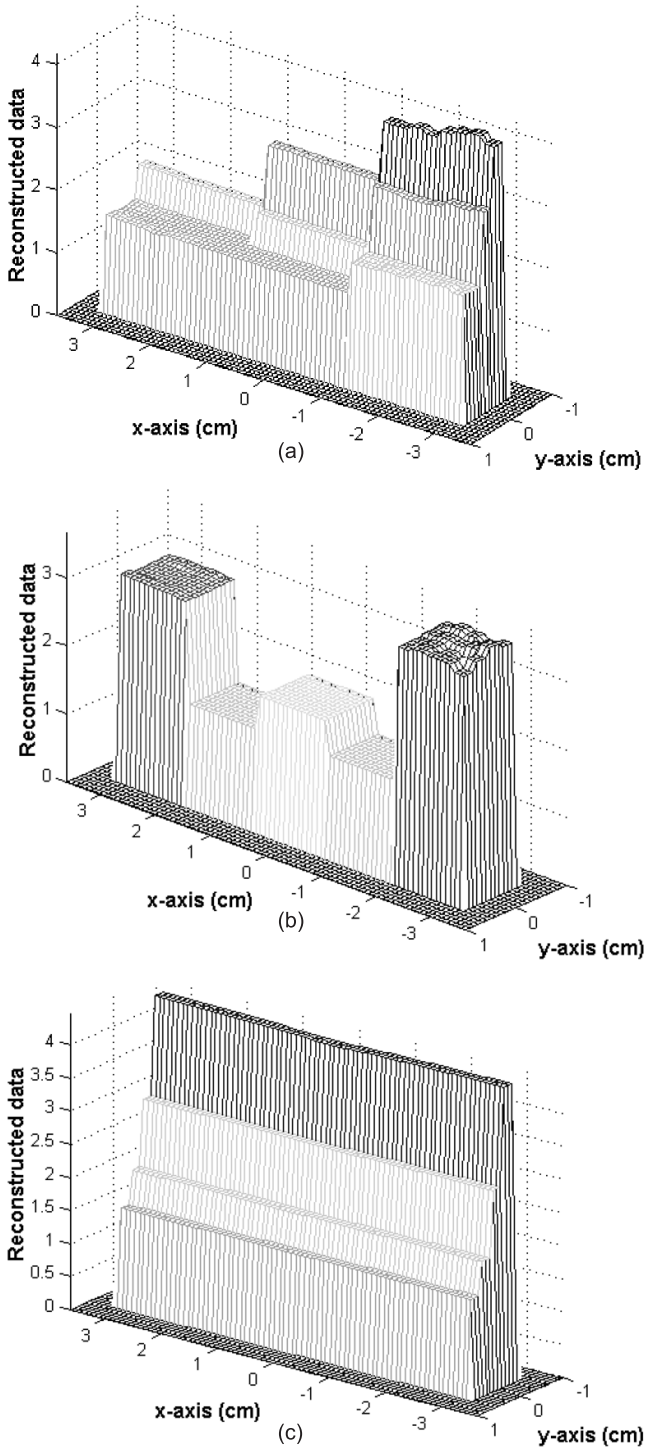

Fig. 3. Reconstructed relative permittivity distribution for example 1, (a)$\varepsilon_a\,(x,y)$, (b)$\varepsilon_b\,(x,y)$, (c)$\varepsilon_c\,(x,y)$.

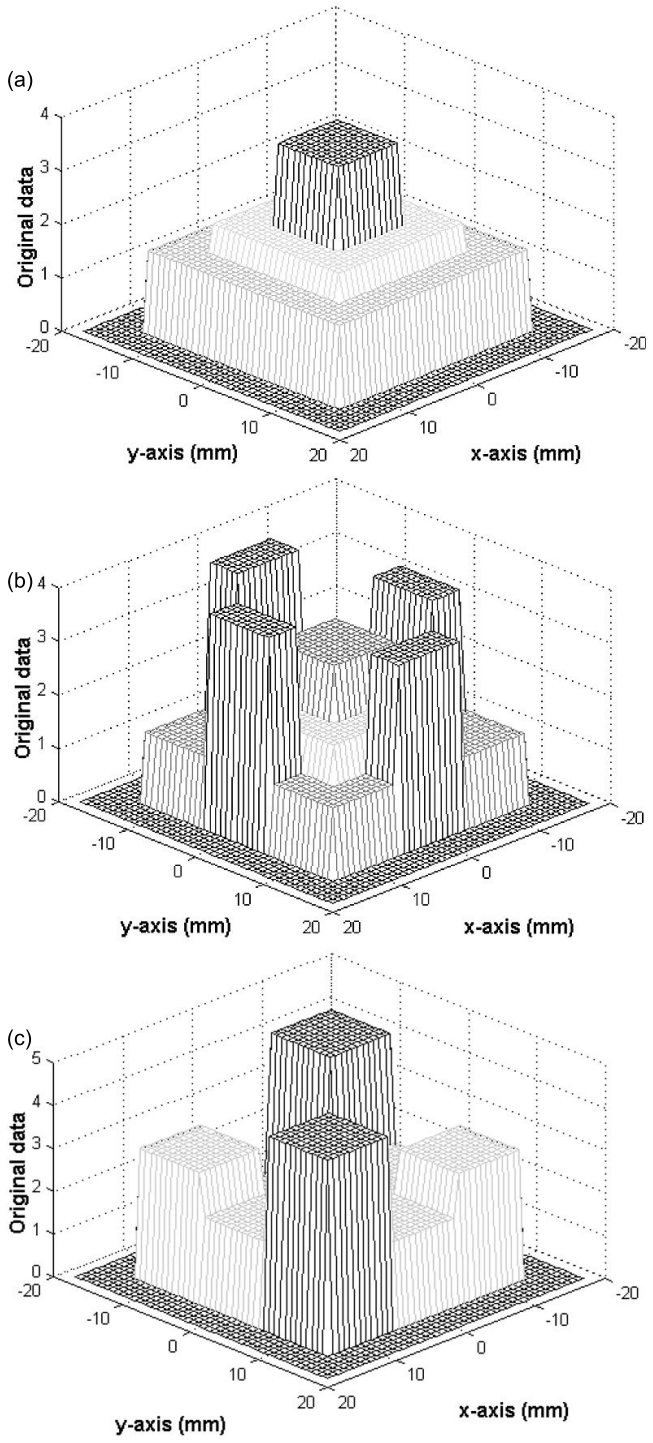

Fig. 4. Original relative permittivity distribution for example 2, (a)$\varepsilon_a\,(x,y)$, (b)$\varepsilon_b\,(x,y)$, (c)$\varepsilon_c\,(x,y)$.

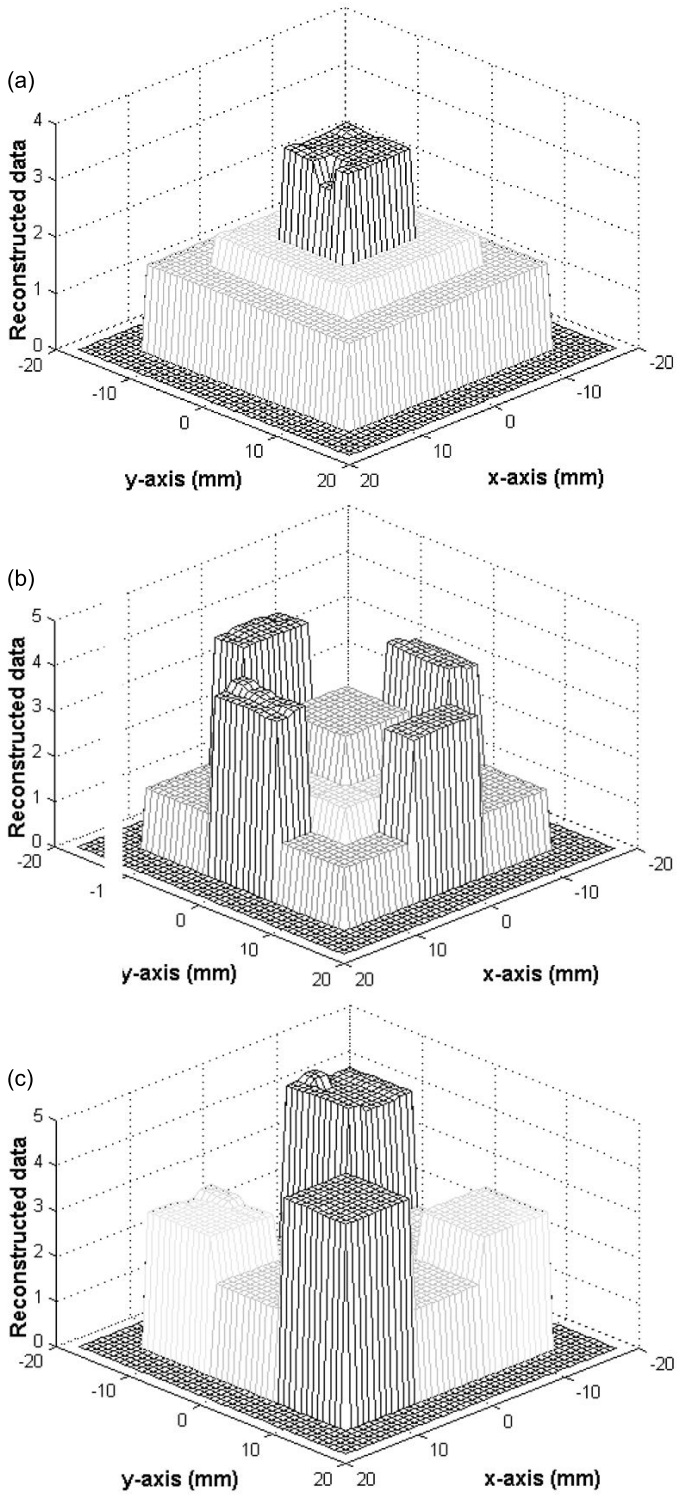

Fig. 5. Reconstructed relative permittivity distribution for example 2, (a)$\varepsilon_a\,(x,y)$, (b)$\varepsilon_b\,(x,y)$, (c)$\varepsilon_c\,(x,y)$.

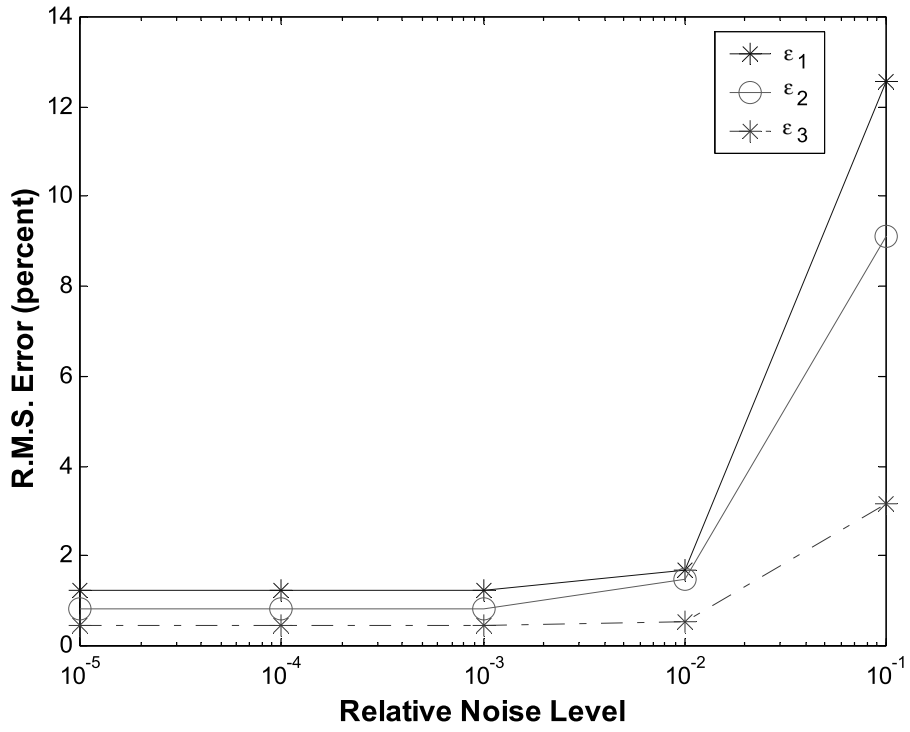

Fig. 6. Reconstructed error as a function of noise level for example 1.

characterized by simple step distribution of permittivity. Each cell has 2.5 mm $\times$ 2.5 mm cross-sections. The reconstructed permittivity distributions of the object are plotted in Fig. 3. The root-mean-square (R.M.S.) error is about 1.2 %, 0.8% and 0.5 % for the dielectric permittivityε_1, ε_2 and ε_3, receptively. It is clear that the reconstruction is good. It is also found the errors for large permittivities are more significant.

In the second example, the buried cylinder with a 27.6 mm $\times$ 27.6 mm square cross section is discretized into 12 $\times$ 12 cells, and the corresponding dielectric permittivities are plotted in Fig. 4. Each cell has 2.3 mm $\times$ 2.3 mm cross-sections. The reconstructed permittivity distributions of the object are plotted in Fig. 5. The R.M.S. error is about 1%, 1% and 1.1% for the dielectric permittivityε_a, ε_b and ε_c, respectively. We can see the reconstruction is also good.

To investigate the effects of noise, we add to each complex scattered field a quantity b+cj, where b and c are independent random numbers having a Gaussian distribution over 0 to the noise level times the R.M.S. value of the scattered field. The noise levels applied are 10^{-5}, 10^{-4}, 10^{-3}, 10^{-2}, and 10^{-1} for the simulations. The numerical results for examples 1 and 2 are plotted in Figs 6 and 7, respectively. They show the effect of noise is tolerable for noise levels below 1%.

Our method depends on the condition number of $[E_z^i]$ and $[E_t^i]$; that is, on having N and 2N unrelated measurements. The procedure will generally not work when the number of unknowns gets very large. This is due to the fact that it is difficult to make such a great number of measurements and make them all unrelated. As a result, the condition number of $[E_z^i]$ and $[E_t^i]$ will become large while the number of unknowns is very large. In such a case, the regularization method should be employed to overcome the ill-posedness. For instance, the pseudoinverse transform techniques [8] can be applied for the inversion of the $[E_z^i]$ and $[E_t^i]$ matrix.

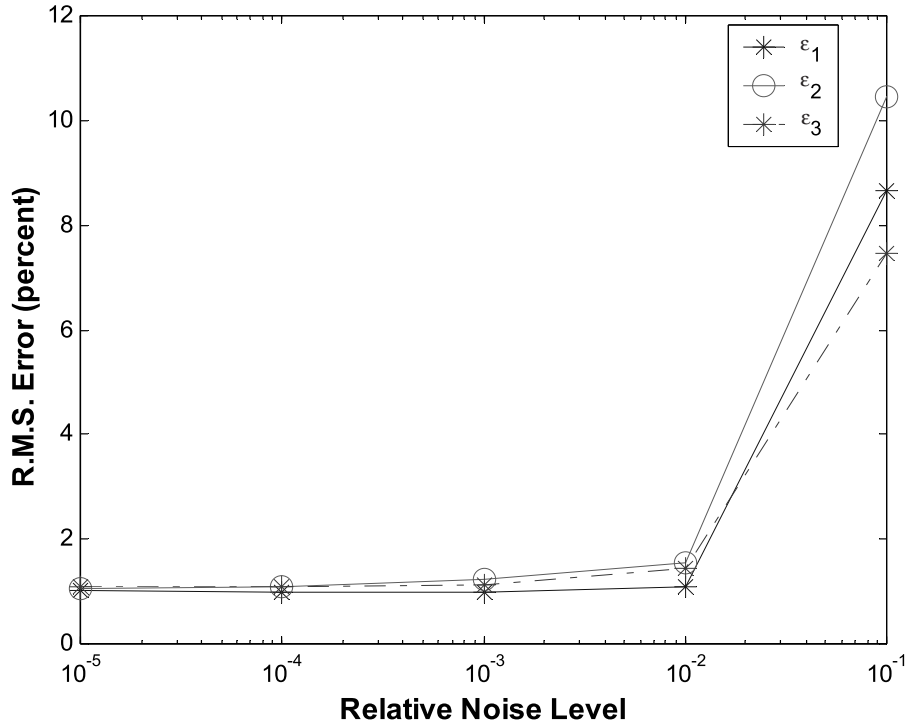

Fig. 7. Reconstructed error as a function of noise level for example 2.

4. Conclusions

An efficient algorithm for reconstructing the permittivity distribution of biaxial dielectric cylinders buried in a slab medium by the knowledge of the scattered field measured outside has been proposed. By properly arranging the direction and the polarization of various unrelated waves, the difficulty of ill-posedness and nonlinearity is avoided. Thus, the permittivity distribution can be obtained by simple matrix operations. The moment method has been used to transform a set of integral equations into matrix form. Then these matrix equations are solved by the unrelated illumination method. Numerical simulation for imaging the permittivity distribution of a buried biaxial dielectric object has been carried out and good reconstruction has been obtained even in the presence of random noise in measured data. This algorithm is very effective and efficient, since no iteration is required.

Appendix

The element in the matrix $[G_1]$ for TM case can be written as

$$(G_1)_{mn} = \left[k_2^2 \cdot \iint_{cell\ n} G_{1s}\left(x, y; x', y'\right) dx' dy' \right] \Bigg|_{\substack{x = x_m \\ y = y_m}}$$

where (x_m, y_m) is the observation point located in the center of the mth cell. For a sufficient small cell, we can replace the cell by a circular cell with the same cross section [20]. Let the equivalent radius of the nth circular cell be a_n. The $(G_1)_{mn}$ can be expressed in the following form

$$(G_1)_{mn} = G_{1s}\left(x_m, y_m; x_n, y_n\right) \cdot k_2^2 \cdot \Delta S_n$$

where (x_n, y_n) is the center of the cell n. ΔS_n denotes the area of the nth cell. Similarly,

$$(G_2)_{mn} = \begin{cases} G_{2ss}\left(x_m, y_m; x_n, y_n\right) \cdot k_2^2 \cdot \Delta S_n + \frac{j\pi k_2 a_n}{2} J_1\left(k_2 a_n\right) H_0^{(2)}\left(k_2 \rho_{mn}\right), & m \neq n \\ G_{2ss}\left(x_m, y_m; x_n, y_n\right) \cdot k_2^2 \cdot \Delta S_n + \frac{j}{2}\left[\pi k_2 a_n H_1^{(2)}\left(k_2 a_n\right) - 2j\right] & m = n \end{cases}$$

with $\rho_{mn} = \sqrt{(x_m - x_n)^2 + (y_m - y_n)^2}$, where J_1 is Bessel function of the first order.

The element in the matrix [G_3] for TE case [21] can be written as

$$(G_3)_{mn} = \left[\left(\frac{\partial^2}{\partial x^2} + k_2^2\right) \cdot \iint_{cell\ n} G_{2s}\left(x, y; x', y'\right) dx' dy'\right]\Bigg|_{\substack{x = x_m \\ y = y_m}}$$

Then $(G_3)_{mn}$ can be expressed in the following form

$$(G_3)_{mn} = \begin{cases} \left.\frac{\partial^2 G_{2ss}(x,y;x_n,y_n)}{\partial x^2}\right|_{\substack{x = x_m \\ y = y_m}} \cdot \Delta S_n + G_{2ss}\left(x_m, y_m; x_n, y_n\right) \cdot k_2^2 \cdot \Delta S_n \\ + \frac{j\pi a_n J_1(k_2 a_n)}{2\rho_{mn}^3}[k_2 \rho_{mn}\left(y_m - y_n\right)^2 H_0^{(2)}\left(k_2 \rho_{mn}\right) + \left((x_m - x_n)^2 - (y_m - y_n)^2\right) \\ \qquad H_1^{(2)}\left(k_2 \rho_{mn}\right)], m \neq n \\ \left.\frac{\partial^2 G_{2ss}(x,y;x_n,y_n)}{\partial x^2}\right|_{\substack{x = x_m \\ y = y_m}} \cdot \Delta S_n + G_{2ss}\left(x_m, y_m; x_n, y_n\right) \cdot k_2^2 \cdot \Delta S_n \\ + \frac{j}{4}\left[\pi k_2 a_n H_1^{(2)}\left(k_2 a_n\right) - 4j\right] \qquad m = n \end{cases}$$

$$(G_4)_{mn} = \begin{cases} \left.\frac{\partial^2 G_{2ss}(x,y;x_n,y_n)}{\partial x \partial y}\right|_{\substack{x = x_m \\ y = y_m}} \cdot \Delta S_n \\ \quad + \frac{j\pi a_n J_1(k_2 a_n)}{2\rho_{mn}^3}\left(x_m - x_n\right)\left(y_m - y_n\right)\left[2H_1^{(2)}\left(k_2 \rho_{mn}\right) - k_2 \rho_{mn} H_0^{(2)}\left(k_2 \rho_{mn}\right)\right], \\ \qquad\qquad m \neq n \\ 0, \qquad\qquad m = n \end{cases}$$

$$(G_5)_{mn} = \begin{cases} \left.\frac{\partial^2 G_s(x,y;x_n,y_n)}{\partial y^2}\right|_{\substack{x=x_m \\ y=y_m}} \cdot \Delta S_n + G_s\left(x_m, y_m; x_n, y_n\right) \cdot k_2^2 \cdot \Delta S_n \\ + \frac{j\pi a_n J_1(k_2 a_n)}{2\rho_{mn}^3}[k_2\rho_{mn}\left(x_m - x_n\right)^2 H_0^{(2)}\left(k_2\rho_{mn}\right) + \left(\left(y_m - y_n\right)^2 - \left(x_m - x_n\right)^2\right) \\ \qquad H_1^{(2)}\left(k_2\rho_{mn}\right) \, m \neq n \\ \left.\frac{\partial^2 G_s(x,y;x_n,y_n)}{\partial y^2}\right|_{\substack{x=x_m \\ y=y_m}} \cdot \Delta S_n + G_s\left(x_m, y_m; x_n, y_n\right) \cdot k_2^2 \cdot \Delta S_n \\ + \frac{j}{4}\left[\pi k_2 a_n H_1^{(2)}\left(k_2 a_n\right) - 4j\right], \qquad m = n \end{cases}$$

$$(G_6)_{mn} = \left.\frac{\partial^2 G_{1s}\left(x, y; x_n, y_n\right)}{\partial x^2}\right|_{\substack{x=x_m \\ y=y_m}} \cdot \Delta S_n + G_{1s}\left(x_m, y_m; x_n, y_n\right) \cdot k_2^2 \cdot \Delta S_n$$

$$(G_7)_{mn} = \left.\frac{\partial^2 G_{1s}\left(x, y; x_n, y_n\right)}{\partial x \partial y}\right|_{\substack{x=x_m \\ y=y_m}} \cdot \Delta S_n$$

$$(G_8)_{mn} = \left.\frac{\partial^2 G_{1s}\left(x, y; x_n, y_n\right)}{\partial y^2}\right|_{\substack{x=x_m \\ y=y_m}} \cdot \Delta S_n + G_{1s}\left(x_m, y_m; x_n, y_n\right) \cdot k_2^2 \cdot \Delta S_n$$

References

[1] S. Caorsi, G.L. Gragnani and M. Pastorino, Numerical electromagnetic inverse-scattering solution for two-dimensional infinite dielectric cylinders buried in a lossy half-space, *IEEE Trans. Antennas Propagat* **AP-41** (Feb 1993), 352–356.

[2] C.C. Chiu and Y.M. Kiang, Inverse scattering of a buried conducting cylinder, *Inv Prob* **7** (Apr 1991), 187–202.

[3] C.C. Chiu and C.P. Huang, Inverse scattering of dielectric cylinders buried in a half space, *Microwave and Optical Technology Letters* **13** (Oct 1996), 96–99.

[4] T.J. Cui and W.C. Chew, Novel diffraction tomographic algorithm for imaging two-dimensional targets buried under a lossy earth, *IEEE Trans. Geosicence and Remote sensing* **38** (Jul 2000), 2033–2041.

[5] T.J. Cui and W.C. Chew, Diffraction tomographic algorithm for the detection of three-dimensional objects buried in a lossy half-space, *IEEE Transactions on Antennas and Propagation* **50** (Jan 2002), 42–49.

[6] O.M. Bucci, L. Crocco, T. Isernia and V. Pascazio, Inverse scattering problems with multifrequency data: reconstruction capabilities and solution strategies, *IEEE Transactions on Geoscience and Remote Sensing* **38** (Jul 2000), 1749–1756.

[7] B. Giovanni, E. Claudio, P. Matteo and R. Andrea, Application of an Inexact-Newton Method Within the Second-Order Born Approximation to Buried Objects, *Ieee Geoscience and Remote Sensing letters* **4** (Jan 2007), 51–55.

[8] M.M. Ney, A.M. Smith and S.S. Stuchly, A solution of electromagnetic imaging using pseudoinverse transformation, *IEEE Trans Med Imag* **MI-3** (Dec 1984), 155–162.

[9] W. Wang and S. Zhang, Unrelated illumination method for electromagnetic inverse scattering of inhomogeneous lossy dielectric bodies, *IEEE Transactions on Antennas and Propagation* **40** (Nov 1992), 1292–1296.

[10] C.P. Chou and Y.W. Kiang, Inverse scattering of dielectric cylinders by a cascaded TE-TM method, *IEEE Transactions on Microwave Theory and Techniques* **47** (Oct 1999), 1923–1930.

[11] G. Leone and F. Soldovieri, Analysis of the distorted born approximation for subsurface reconstruction: truncation and uncertainties, *IEEE Transactions on Geoscience and Remote Sensing* **41** (Jan 2003), 66–74.

[12] F. Soldovieri and R. Persico, Reconstruction of an Embedded Slab from Multifrequency Scattered Field Data under the Distorted Born Approximation, *IEEE Transactions on Antennas and Propagation* **52** (Sept 2004), 2348–2356.
[13] V.A. Mikhnev and P. Vainikainen, Two-Step Inverse Scattering Method for One-Dimensional Permittivity Profiles, *IEEE Transactions on Antennas and Propagation* **48** (Feb 2000), 293–298.
[14] K.A. Nabulsi and D.G. Dudley, A New Approximation and a New Measurable Constraint for Slab Profile Inversion, *IEEE Transactions on Geoscience and Remote Sensing* **34**(3) (May 1996).
[15] Y.S. Lin and C.C Chiu, Image Reconstruction for a Perfectly Conducting Cylinder Buried in Slab Medium by a TE Wave Illumination, *Electromagnetics* (3) (April 2005), 203–216.
[16] C.J. Lin, C.Y. Chou and C.C. Chiu, Electromagnetic Imaging for a Conducting Cylinder Buried in a Slab Medium by the Genetic Algorithm, *International Journal of Imaging Systems and Technology* **14** (June 2004), 1–7.
[17] C.C. Chiu, Inverse scattering of inhomogeneous biaxial materials coated on a Conductor, *IEEE Transactions on Antennas and Propagation* **46** (Feb 1996), 218–225.
[18] A. Ishimaru, Electromagnetic Wave Propagation, Radiation and Scattering, *Englewood Cliffs, NJ: Prentice-Hall*, 1991.
[19] R.F. Harrington, Field Computation by Moment Methods, *New York: Macmillan*, 1968.
[20] J.H. Richmond, Scattering by a dielectric cylinder of arbitrary cross section shape, *IEEE Transactions on Antennas and Propagation* **13** (May 1965), 334–341.
[21] J.H. Richmond, TE-wave scattering by a dielectric cylinder of arbitrary cross-session shape, *IEEE Transactions on Antennas and Propagation* **14** (July 1966), 460–464.